BIOCELL

Tech Science Press

http://doi.org/10.32604/biocell.2026.077349

ARTICLE

Mitochondrial Calcium Uniporter (MCU) Inhibition Disrupts Bone Remodeling and Impairs Mitochondrial Function via Aberrant Mitochondrial Dynamics

Xinliang Fu[1,#], Wen Du[1,#], Tao Li[2], Yifei Shen[1], Ngai-Fung Ruan[1], Huiling Ling[1], Xingbo Wu[1], Ziqi Qin[1], Xiting Zhu[1] and Xueqi Gan[1,*]

[1]State Key Laboratory of Oral Diseases & National Center for Stomatology & National Clinical Research Center for Oral Diseases, West China Hospital of Stomatology, Sichuan University, Chengdu, China

[2]Department of Anesthesiology, Laboratory of Mitochondrial Metabolism and Perioperative Medicine, National Clinical Research Center for Geriatrics, West China Hospital of Sichuan University, Chengdu, China

*Corresponding Author: Xueqi Gan. Email: xueqigan@scu.edu.cn

#These authors contributed equally to this work

Received: 08 December 2025; Accepted: 09 April 2026; Published: 29 June 2026

ABSTRACT: Objectives: Mitochondrial function is intricately linked to osteogenic and osteoclastic differentiation. The mitochondrial calcium uniporter (MCU) is a critical regulator of mitochondrial function, influencing key aspects of cellular metabolism and signaling. However, the precise mechanisms by which MCU modulates osteogenic activity remain unclear. This study aimed to elucidate the impact of MCU-mediated regulation of mitochondrial function on bone remodeling and to explore the underlying mechanisms. **Methods:** The mouse pre-osteoblastic cells (MC3T3-E1) were treated with the MCU-specific inhibitor Ru265 during osteogenic induction to assess changes in osteogenic differentiation capacity, mitochondrial function, and mitochondrial dynamics. Additionally, MCU global knockout (MCU KO) mice were employed as an *in vivo* model to explore the role of MCU in bone structure phenotype through bone microstructural analysis and histological examination. **Results:** Quantitative reverse transcription (qRT) PCR, western blotting, alizarin Red-S (ARS) staining, and alkaline phosphatase (ALP) activity analyses revealed that the inhibition of MCU function by Ru265 downregulates ALP activity (about 59.60% of the control group) and the expression of osteogenic markers in MC3T3-E1 cells. Dramatically increased dynamin-related protein 1 (Drp1) expression (about 1.13 times of the control group), decreased mitofusion-2 (Mfn2) expression (about 14.51% of the control group), and reduced mitochondrial membrane potential (MMP) (about 55.16% of the control group) were observed, all indicating substantial disruption of mitochondrial dynamics and function in MC3T3-E1 cells. The corroborating evidence is that μCT and histological analyses of MCU global knockout mice revealed impaired osteogenic differentiation, reduced bone mass formation, and deteriorated trabecular bone microstructure compared with wild-type mice. **Conclusion:** MCU inhibition elicits aberrant mitochondrial dynamics and mitochondrial dysfunction, thereby impairing osteogenic function and disrupting bone remodeling, which could have promising implications for bone metabolism.

KEYWORDS: Mitochondrial calcium uniporter (MCU); mitochondrial dynamics; mitochondrial functions; bone remodeling; osteogenic function

1 Introduction

The bone is a multifunctional organ undergoing continuous remodeling. In healthy adults, skeletal homeostasis is maintained through a precise balance between bone formation by osteoblasts and bone

Copyright © 2026 The Authors. Published by Tech Science Press. This work is licensed under a Creative Commons Attribution 4.0 International License, which permits unrestricted use, distribution, and reproduction in any medium, provided the original work is properly cited.

resorption by osteoclasts. Therefore, studying the mechanisms of osteoblast differentiation and functional activities of is essential for understanding bone physiology and bone pathology, and for investigating therapies to promote bone repair and regeneration [1,2].

It is widely acknowledged that mitochondria are not merely the "energy station" of cells, but also the integration platform for multi-signal cascades in response to the body's stress injury [3–5]. The modulation of mitochondrial functions, including the mitochondrial outer membrane permeability, is pivotal in regulating bone remodeling [6,7]. Mitochondrial dysfunction has been linked to compromised osteogenesis, enhanced osteoclast activity, accelerated age-related bone loss [8], aggravated chondrocyte apoptosis and cartilage matrix pathological calcification in the development of osteoarthritis [9], and increased bone resorption in diabetic periodontitis [10]. Previous studies demonstrated that regulation of mitochondrial function and mitophagy by Sirtuin3 signaling promotes osteogenic differentiation [11] and modulates BMSC aging and senile osteoporosis induced by advanced glycation end products (AGEs) [12].

Being highly dynamic organelles, mitochondria undergo constant fusion and fission processes. Mitochondria are highly dynamic organelles maintained through continuous cycles of fusion and fission. This balance in mitochondrial dynamics is closely linked to mitochondrial functional status and plays a critical role in both cellular physiological and pathological processes [13–15]. There is abundant evidence that indicates that bone damage and many diseases associated with imbalanced bone homeostasis are accompanied by varying degrees of mitochondrial dynamics imbalance [16–18]. A key regulator of this process is dynamin-related protein 1 (Drp1), which is translocated from the cytoplasm to the mitochondrial outer membrane under stress conditions to execute mitochondrial fission. Under oxidative stress or inflammatory stimulation, Drp1 upregulation drives excessive mitochondrial fission in osteoblasts, impairing oxidative phosphorylation, elevating reactive oxygen species (ROS) production, and ultimately compromising osteogenic differentiation [19–21]. In addition, excessive mitochondrial fission can increase mitochondrial membrane permeability, thereby releasing multiple damage-related factors (such as damage-associated molecular patterns, DAMPs) and accelerating bone damage [22]. On the other hand, mitofusin 2 (Mfn2), located on the outer mitochondrial membrane, mediates mitochondrial fusion—facilitating the energy and information transfer between different mitochondria, the rapid transmission of mitochondrial membrane potential, and the exchange and complementation of mitochondrial content and mitochondrial genome (mitochondrial DNA, mtDNA) [23,24]. Mfn2 regulates osteoclast differentiation by regulating the Ca^{2+}-nuclear factor of activated T cells 1 (NFATc1) axis [16]. Icariin safeguards BMSCs from iron overload-induced injury by regulating mitochondrial dynamics and intervening in PI3K/AKT/mTOR and MAPK pathways [25]. These findings collectively highlight mitochondrial dysfunction as a central player in bone injury and point to key mitochondrial proteins as promising targets for restoring osteogenic capacity in bone-related disorders.

The mitochondrial calcium uniporter (MCU), situated in the inner mitochondrial membrane, mediates unidirectional calcium uptake into the mitochondrial matrix and is closely linked to cellular life activities by regulating mitochondrial function and dynamics. Many pathological responses of the body, such as myocardial ischemia-reperfusion injury and diabetic kidney injury, are accompanied by abnormal MCU function, which is a potential therapeutic target [26,27]. Studies have demonstrated that MCU-mediated modulation of mitochondrial function is closely linked to metabolic abnormalities-induced arrhythmias [28] and contributes to the alleviation of muscle injury [29]. Recently, the regulatory role of MCU in mitochondrial dynamics has garnered significant research attention. Differences in MCU expression across neuronal cell types and circuits tune mitochondrial morphology to meet distinct synaptic demands, stress injury, leading to excessive mitochondrial fission [30]. Furthermore, MCU is involved in cancer-related biological

effects by regulating mitochondrial calcium homeostasis and mitochondrial dynamics [31]. MCU inhibition relieves intestinal ischemia–reperfusion injury by suppressing Drp1-dependent mitochondrial fission [32]. However, the specific regulatory mechanism of MCU on mitochondrial function and dynamics remains unclear, and whether this process plays a role in bone remodeling has rarely been reported.

Herein, taking the foregoing considerations into account, we applied the MCU-specific inhibitor Ru265 during osteogenic differentiation of MC3T3-E1 cells to detect the changes in osteogenic function, mitochondrial function, and mitochondrial dynamics. Additionally, bone microstructural and histological analysis were performed on MCU global knockout mice to investigate the effects and mechanisms of MCU-regulated mitochondrial functions and mitochondrial dynamics on osteogenic function and bone remodeling. This study could offer new insights into the development of bone regeneration and repair therapies targeting MCU and key mitochondrial function proteins.

2 Materials and Methods

2.1 Animals

All animal procedures were approved by the Research Ethics Committee of West China Hospital of Stomatology (Approval No. WCHSIRB-D-2022-271). The study utilized forty mice in two groups (twenty mice per group): wild-type group (WT) and MCU global knockout group (MCU KO) (Fig. A1), which were derived from a mixed genetic background of C57BL/6 and CD1 strains (6–8 weeks old, male, 20–25 g, specific pathogen-free) as described [33]. These mice were kindly provided by the National Institutes of Health (Bethesda, MD, USA) to the Laboratory of Mitochondrial Metabolism and Perioperative Medicine, West China Hospital of Sichuan University, where they were subsequently transferred by Professor Tao Li for this study. The mice were kept under controlled environmental conditions and maintained on a standard laboratory diet with free access to water. Euthanasia was performed by administering an overdose of 2% (20 mg/mL) sodium pentobarbital solution via intraperitoneal injection. Following euthanasia, femurs and tibias were harvested sterilely for histomorphological and histochemical analyses.

2.2 Cell Culture and Treatment

Mouse pre-osteoblastic cells (MC3T3-E1, Cat# BNCC360180, RRID: CVCL_0409; Beina Chuanglian Biotechnology Institute, Beijing, China), generously provided by the State Key Laboratory of Oral Diseases of Sichuan University, have undergone STR identification and are free of mycoplasma contamination. The cells were cultured using α-MEM (Cat#C12571500BT, Gibco, Grand Island, NY, USA) supplemented with 10% fetal bovine serum (Cat#10099-141, Gibco, Melbourne, Australia) and 1% penicillin-streptomycin (Cat#15140-122, Gibco, USA). All cultures were maintained at 37°C in a 5% CO_2 humidified incubator with medium renewal every two days. For experimentation, cells were seeded in 24-well plates at a density of 1.5×10^4 cells per well. Upon reaching approximately 90% cell confluence, the growth medium was substituted with osteogenic induction medium, containing 10 mmol/L β-glycerophosphate disodium, 50 μg/mL ascorbic acid, and 100 nmol/L dexamethasone. Ru265, a specific inhibitor of mitochondrial calcium uptake (MCU), was used to treat the cells. The MC3T3-E1 cells were allocated to two groups: the control group (MC3T3-E1) treated with phosphate-buffered saline (PBS, pH 7.2 (1×), components: potassium phosphate monobasic (KH_2PO_4) 210.0 mg/L, sodium chloride (NaCl) 9000.0 mg/L, sodium phosphate dibasic ($Na_2HPO_4{\cdot}7H_2O$) 726.0 mg/L; Cat#C20012500BT, Gibco), and the MCU inhibition group (MC3T3-E1 + Ru) treated with Ru265 (10 μmol/L; Cat#SML2991, Sigma-Aldrich, St. Louis, MO, USA) in both the growth and osteogenic induction media. Treatments were sustained throughout the culture period until biochemical and molecular assays were performed.

2.3 Cell Viability

MC3T3-E1 cells were seeded in 96-well plates at a density of 5×10^3 cells/well, and growth medium containing different concentrations of Ru265 was added to each group. After 24 h of treatment, 10 μL of Cell Counting Kit-8 (CCK-8) working solution (Cat#K1018, APExBIO, Houston, TX, USA) was added to each well, and the plate was gently shaken for 10 s to ensure the compounds in the wells well-mixed. After incubation for 3 h at 5% CO_2 and 37°C in a cell culture incubator protected from light, the 96-well plate was taken out. The OD value of the supernatant was measured at λ = 450 nm.

2.4 Alkaline Phosphatase (ALP) Activity Assay

After 7-day osteogenic induction, 30 μL of cell lysis buffer (without proteinase phosphatase inhibitors; Cat#P0013, Beyotime, Shanghai, China) was added to each well. Cells were gently pipetted to ensure complete lysis, and the resulting lysate was transferred to enzyme-free EP tubes. These samples were centrifuged at 10,000× *g* for 5 min at 4°C, after which the supernatant was collected for analysis of alkaline phosphatase (ALP) activity using an Alkaline Phosphatase Assay Kit (Cat#P0321S, Beyotime). Absorbance was measured at 405 nm using a microplate reader (Varioskan LUX, Thermo Scientific, Waltham, MA, USA).

2.5 ALP Staining

Following 7 days of osteogenic induction, MC3T3-E1 cells were rinsed with PBS (pH 7.2 (1×)) and fixed with 4% paraformaldehyde (Cat#BL539A, Biosharp, Hefei, China) for 10 min at room temperature. Alkaline phosphatase (ALP) activity was assessed using a BCIP/NBT staining kit (Cat#C3206, Beyotime) according to the manufacturer's instructions, with incubation carried out for 24 h. After a final PBS wash, stained cultures were scanned using an Epson Perfection V370 Photo Scanner (Nagano, Japan) for image acquisition.

2.6 Alizarin Red-S (ARS) Staining

After 14 days of osteogenic induction, mineralized nodules in MC3T3-E1 cells were visualized by staining with 1% Alizarin Red S (Cat#G1452, pH 4.2; Solarbio, Beijing, China) for 5 min, following fixation with 4% PFA for 15 min and PBS (pH 7.2 (1×)) washing. The stained cells were then gently washed with ultra-pure water and subsequently scanned with an Epson Perfection V370 Photo Scanner. Quantification was performed by dissolving mineralized nodules in 10% cetylpyridinium chloride (Cat#HY-B1464R, MedChemExpress, Monmouth Junction, NJ, USA) for 30 min prior to absorbance measurement at 562 nm with a microplate reader (Thermo Scientific).

2.7 Mitochondrial Morphology Observation

MitoTracker Red (Cat# M7512, Invitrogen, Carlsbad, CA, USA) was used to observe mitochondrial morphology in MC3T3-E1 cells, adhering to the manufacturer's guidelines. The control group (MC3T3-E1) was treated with PBS (pH 7.2 (1×)), and the MCU inhibition group (MC3T3-E1 + Ru) was treated with Ru265 (10 μmol/L) in the growth media for 24 h. After treatment, cells were washed with PBS (pH 7.2 (1×)), followed by incubation in serum-free α-MEM containing 100 nmol/L MitoTracker Red at 37°C for 30 min. Subsequently, cells were fixed with 4% PFA, and fluorescent images were acquired using a Laser Scanning Confocal Microscope (LSCM, OLYMPUS FV3000, Tokyo, Japan) with an excitation wavelength of 599 nm for MitoTracker Red. Mitochondrial morphology was quantitatively analyzed using the Mitochondrial Network Analysis (MiNA) and Mito Analyzer plugins within ImageJ software (1.8.0, NIH, USA).

2.8 Determination of Mitochondrial Membrane Potential (MMP)

Mitochondrial membrane potential (MMP) was detected using tetramethylrhodamine methyl ester (TMRM; Cat#I34361, Invitrogen), a potentiometric fluorescent dye. MC3T3-E1 cells were co-stained with MitoTracker Green (100 nmol/L; Cat#M7514, Invitrogen) and tetramethylrhodamine methyl ester (TMRM, 100 nmol/L; Cat#I34361, Invitrogen) for 30 min at 37°C to simultaneously visualize mitochondria and their membrane potential. Fluorescent images were acquired by laser scanning confocal microscopy (LSCM) using excitation wavelengths of 543 nm (TMRM) and 488 nm (MitoTracker Green). Fluorescent intensity was quantified using ImageJ software (1.8.0, NIH, USA). The MMP data were normalized by calculating the ratio of red (TMRM) to green (MitoTracker Green) fluorescence intensity for each group to rule out the possibility of the low TMRM signal due to low mitochondrial mass.

2.9 Quantitative Reverse Transcription (qRT) PCR

Following the isolation of total RNA using the FastPure® Cell/Tissue Total RNA Isolation Kit V2 (Cat#RC112, Vazyme, Nanjing, China) according to the manufacturer's protocol, RNA concentration and purity were assessed spectrophotometrically (NanoPhotometer® NP80, Implen, Munich, Germany). cDNA was then reverse-transcribed with the HiScript III All-in-one RT SuperMix for qPCR (Cat#R333, Vazyme). Amplification was carried out using the ABI PRISM 7300 Real-Time PCR System (Applied Biosystems, Foster City, CA, USA) with Taq Pro Universal SYBR qPCR Master Mix (Cat#Q712, Vazyme) and gene-specific primers (Table 1) in a 20 μL reaction volume. Relative gene expression (*Mcu*, *Micul*, *ALP*, *OCN*) normalized to housekeeping gene Gapdh was calculated using the $2^{-\Delta\Delta CT}$ method.

Table 1: Primer sequences for qRT-PCR analysis of the mRNA expression.

Genes	Forward Primer (5′-3′)	Reverse Primer (5′-3′)
Mcu	GATGACGTGACGGTGGTTTA	GTCAGAGATAGGCTTGAGTGTG
Micu1	ACACCCTCAAGTCTGGCTTAT	TTCCCATCTTTGAAGTGCTTCTT
ALP	CCAACTCTTTTGTGCCAGAGA	GGCTACATTGGTGTTGAGCTTTT
OCN	GAACAGACTCCGGCGCTA	AGGGAGGATCAAGTCCCG
Gapdh	ACTTTGTCAAGCTCATTTCC	TGCAGCGAACTTTATTGATG

2.10 Western Blotting

Protein lysates were prepared from cultured cells using Cell Lysis Buffer (Cat#P0013, Beyotime) following the manufacturer's protocol. Protein concentration was determined with a BCA assay kit (Cat#P0010S, Beyotime). Equal amounts of protein were separated by 10% SDS-PAGE (BeyoGel™ Plus Precast Gel, Cat#P0456S, Beyotime) and transferred to PVDF membranes (Cat#1620184, Bio-Rad, Hercules, CA, USA). After blocking with QuickBlock™ Buffer (Cat#P0252, Beyotime), membranes were incubated overnight at 4°C with the following primary antibodies: anti-Runx2 (1:1000, Cat#AF5186; Affinity, Liyang, China), anti-ALP (1:1000, Cat#DF6225; Affinity), anti-Drp1 (1:3000, Cat#PA5-20176; Thermo Fisher Scientific, Waltham, MA, USA), anti-Mfn2 (1:1000, Cat#M6319; Sigma-Aldrich), and anti-β-actin (1:8000, Cat#ab6276; Abcam, Cambridge, UK). Following incubation with HRP-conjugated secondary antibodies, either goat anti-mouse IgG H&L polyclonal antibody (1:10,000, Cat#ab6789; Abcam) or goat anti-rabbit IgG H&L polyclonal antibody (1:10,000, Cat#ab6721; Abcam), protein bands were visualized using chemiluminescence (ChemiDoc™ MP Imaging System, Cat#12003154, Bio-Rad). Band intensities were quantified with ImageJ software (v1.8.0, NIH, USA), with β-actin as the loading control.

2.11 μCT and Histomorphometric Analysis

Following fixation in 10% formaldehyde for 72 h, the metaphyseal regions of femurs and tibiae were scanned using a μCT 50 system (SCANCO Medical, Brüttisellen, Switzerland) under the following parameters: 90 kV and 114 mA energy, 300 ms integration time, and 10 μm isotropic voxel size. Upon reconstruction and analysis of raw images with SCANCO Medical software (SCANCO Visualizer 1.1.18.0, SCANCO Evaluation 1.1.19.0; SCANCO Medical, Brüttisellen, Switzerland), a cylindrical volume of interest (VOI) was defined, spanning 150 slices (1.5 mm) towards the bone marrow, starting 1.0 mm below the cortex. The microstructural parameters were quantified within the VOI: bone volume fraction (BV/TV), trabecular number (Tb.N), trabecular thickness (Tb.Th), and trabecular separation (Tb.Sp).

2.12 Hematoxylin and Eosin (H&E), Immunohistochemistry (IHC), and Tartrate-Resistant Acid Phosphatase (Trap) Staining

After μCT analysis, bone samples were decalcified, dehydrated through an ascending ethanol series, infiltrated, and embedded in paraffin. Following preparation of 4-μm-thick sections with a rotary microtome (RM2016, Leica, Wetzlar, Germany), the deparaffinization of sections was carried out using BioDewax and Clear Solution (Cat#G1128, Servicebio, Wuhan, China). The bone tissue slices were then subjected to Hematoxylin and Eosin (H&E), immunohistochemistry (IHC), and tartrate-resistant acid phosphatase (TRAP) staining, respectively. Images were captured using a panoramic tissue section scanner (WS-10, Wisleap, Changzhou, China).

For H&E staining, the sections were stained with Hematoxylin and Eosin using a HE dye solution kit (Cat#G1003, Servicebio) according to the product manual, dehydrated, and mounted with neutral resin (Cat#10004160, Sinopharm Group Chemical Reagent Co., Ltd., Shanghai, China).

For IHC staining, bone tissue sections were subjected to antigen retrieval using heated citrate buffer (pH 6.0) and then cooled to room temperature. Endogenous peroxidase activity was quenched with 3% hydrogen peroxide solution, and antigen retrieval was performed with 3% BSA for 30 min to minimize nonspecific binding. Primary antibodies against RUNX2 (1:200, Cat#AF5186; Affinity), ALP (1:200, Cat#DF6225; Affinity), BMP2 (1:200, Cat#AF5163; Affinity), and OPG (1:200, Cat#DF6824; Affinity) were applied and incubated overnight at 4°C. Following incubation with secondary anti-mouse IgG antibodies (1:200, Cat#S0002; Affinity), the primary antibody was detected using a DAB-horseradish peroxidase substrate system (Cat#G1212, Servicebio) for visualization.

For TRAP staining, deparaffinization was performed with BioDewax and Clear Solution, followed by rehydration. The sections were stained using the TRAP staining kit (Cat#G1050, Servicebio). Briefly, the slides were incubated in distilled water in a wet box at 37°C for 2 h. Freshly prepared and filtered TRAP incubation solution was then applied and incubated for 20 min at 37°C. After incubation, the TRAP solution was removed, and the sections were washed before re-staining the nuclei with hematoxylin solution (Cat#G1004, Servicebio) for 15 s. Differentiation was carried out with differentiation fluid, followed by ammonia (Cat#G1040, Servicebio) to return the sections to blue. Finally, the slides were dehydrated and mounted.

2.13 Statistical Analysis

The data are presented as means (of fold increase) ± standard deviations (SDs). Statistical analyses were conducted using GraphPad Prism 9.3 software (Graphpad Software, Inc., La Jolla, USA). Prior to multiple groups' comparisons, the normality of data in each group was assessed using the Shapiro-Wilk test. Homogeneity of variances across groups was tested using the Brown-Forsythe test. For data meeting both assumptions, one-way ANOVA was performed, followed by Tukey's post hoc test for multiple comparisons

if the ANOVA was significant. Differences between the two independent groups were assessed using unpaired *t*-tests. The normality of data was verified using the Shapiro-Wilk test, and homogeneity of variances was assessed using an F test. For data meeting the normality assumption, Student's *t*-test was used when variances were equal; otherwise, Welch's corrected *t*-test was applied. $p < 0.05$ was considered statistically significant.

3 Results

3.1 MCU Functional Inhibition Upregulates the Expression of Mcu and Micu1 Genes in the Early Stage of Osteogenic Differentiation of MC3T3-E1 Cells

Mitochondrial calcium uptake 1 (MICU1) is one of the MCU functionally related regulatory proteins located on the outer surface of the inner mitochondrial membrane (IMM), facing the intra-membrane gap [34]. As shown in Fig. 1A, the expression level of the *Mcu* gene in MC3T3-E1 cells was significantly increased after 72 h of osteogenic differentiation compared to that of non-osteogenic differentiation (0 h). The gene expression level of *Micu1* was also dramatically increased after 48 h and 72 h of osteogenic differentiation in MC3T3-E1 cells (Fig. 1B). Furthermore, the cells were treated with PBS or MCU pharmacological inhibitor Ru265 (10 μmol/L). In contrast to the control group (MC3T3-E1), the *Mcu* gene expression levels were markedly higher in the MCU-inhibition group (MC3T3-E1 + Ru) after 24 h and 72 h of osteogenic differentiation (Fig. 1C). After 72 h of osteogenic differentiation induction, the gene expression level of *Micu1* was also significantly elevated in the MCU functional inhibition group (Fig. 1D).

Following 7 days of osteogenic differentiation, the expression levels of *Mcu* and *Micu1* genes in MC3T3-E1 cells were also remarkably increased compared to those of non-osteogenic differentiation (0 d) (Fig. A2A,B). Subsequent experiments involved treating cells with either PBS or Ru265 (10 μmol/L). After 7 days of differentiation, the MCU-inhibition group (MC3T3-E1 + Ru) displayed significantly elevated *Mcu* transcript level compared to the control group (MC3T3-E1) (Fig. A2C). A similar increase in *Micu1* expression was noted in the MCU-inhibition group following the 7-day induction period (Fig. A2D), albeit without reaching statistical significance.

Examination of Fig. A3A reveals that *Mcub* gene expression in MC3T3-E1 cells rose significantly at 24 h post-osteogenic induction relative to non-osteogenic differentiation (0 h). Transcript levels of *Mcur1* also trended upward at 24, 48, and 72 h post-induction (Fig. A3B), though these changes did not achieve statistical significance. Compared to the control group (MC3T3-E1), the MCU-inhibition group (MC3T3-E1 + Ru) exhibited significantly higher *Mcub* expression after 72 h of differentiation (Fig. A3C). A similar, albeit non-significant, elevation in *Mcur1* gene expression was also observed in the MCU-inhibition group at the 72-h time point (Fig. A3D).

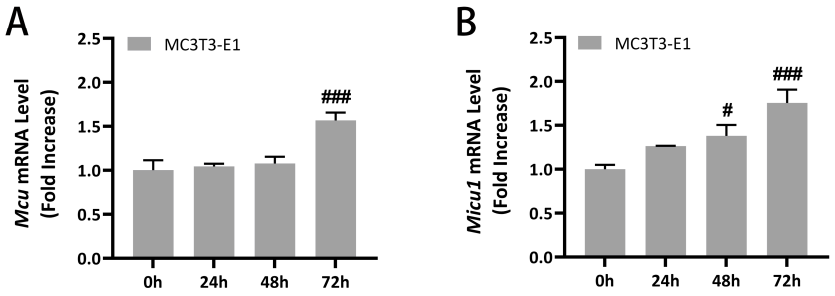

Figure 1: *Cont.*

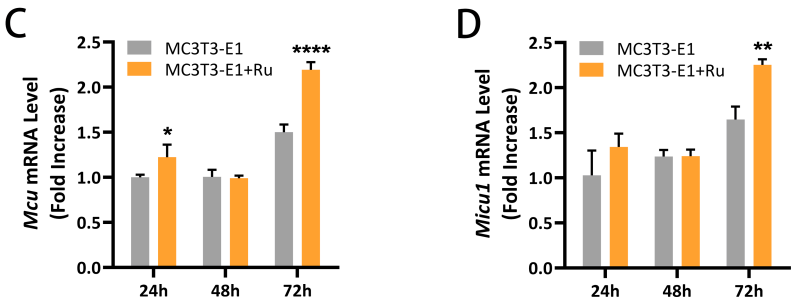

Figure 1: The effect of abnormal MCU function on the expression of MCU-related genes in the early stage of osteogenic differentiation of MC3T3-E1 cells. (**A**,**B**) mRNA expression level of *Mcu* and *Micu1* gene of MC3T3-E1 cells after osteogenic differentiation induction for 0 h, 24 h, 48 h, and 72 h. (**C**,**D**) mRNA expression level of *Mcu* and *Micu1* gene of the control group (MC3T3-E1) and the MCU function inhibition group (MC3T3-E1 + Ru) after osteogenic differentiation induction for 0 h, 24 h, 48 h, and 72 h. Results are shown as means of fold increase ± SDs. $^{\#}p < 0.05$ and $^{\#\#\#}p < 0.001$ versus the undifferentiated group (0 h); $^{*}p < 0.05$, $^{**}p < 0.01$ and $^{****}p < 0.0001$ versus the control group (MC3T3-E1), n = 5.

3.2 Inhibition of MCU Function Impairs Osteogenic Functions of MC3T3-E1 Cells

The early osteogenic function of MC3T3-E1 cells was evaluated using ALP staining and quantitative activity analysis, a well-established early marker of osteogenic differentiation [35]. The incompetent osteogenic differentiation ability of MCU inhibited MC3T3-E1 cells (MC3T3-E1 + Ru) was evidenced by shallower ALP staining (Fig. 2A) and weaker ALP activity (Fig. 2B). The calcium nodule formation, a pivotal biomarker of osteogenic differentiation, was assessed by Alizarin Red-S (ARS) staining after 14 days of osteogenic differentiation induction [36]. Semi-quantitative analysis revealed less calcium mineralization in the MCU-inhibition group (Fig. 2C,D). To corroborate this, we proceeded to examine the expression levels of pivotal osteogenic markers, assessing both mRNA and protein. There is downregulated gene expression of osteogenic markers, including *ALP* and *OCN* (Fig. 2E,F), and decreased protein expression of osteogenic markers, including RUNX2 and ALP (Fig. 2G,H), in MCU-inhibited MC3T3-E1 cells. These results demonstrate that inhibition of MCU function by Ru265 impairs the osteogenic functions of MC3T3-E1 cells. Given that MCU-mediated modulation of mitochondrial function and dynamics is closely linked to many pathological responses, we speculated that MCU-induced cellular osteogenic dysfunction may be associated with mitochondrial dysfunction and abnormal mitochondrial dynamics.

3.3 Inhibition of MCU Function Induces Abnormal Mitochondrial Dynamics and Mitochondrial Dysfunction in MC3T3-E1 Cells

We next sought to investigate whether mitochondrial function and dynamics are actually changed after MCU inhibition in this study. MC3T3-E1 cells were treated with different concentrations of Ru265, and their effects on cell activity were examined by CCK-8 assay. Cell activity was significantly reduced at concentrations higher than 50 μM (Fig. 3A). Combined with the published literature, 10 μM was selected as the appropriate concentration. Given that normal mitochondrial structure and morphology underpins functional performance [37] and is regulated by key proteins such as Mfn2 and Drp1 [38], we first performed the qRT-PCR analysis and western blot to assess their expression in the control group (MC3T3-E1) and the MCU-inhibited group (MC3T3-E1 + Ru) during osteogenic differentiation. As shown in Fig. 3B, compared with the control group, Mfn2 protein expression level was distinctly downregulated in the MCU-inhibited group after 7 days of osteogenic differentiation. Conversely, Drp1 protein expression level was notably upregulated in the MCU-inhibited group relative to the control group after 14 days of osteogenic differentiation (Fig. 3C). In

the MCU-inhibition group, the expression trend of the *Mfn2* gene after 7 days of differentiation was consistent with that of Mfn2 protein (Fig. 3D). Additionally, a significant upregulation in *Drp1* gene expression was observed at day 14 (Fig. 3E), which mirrored the change in Drp1 protein expression.

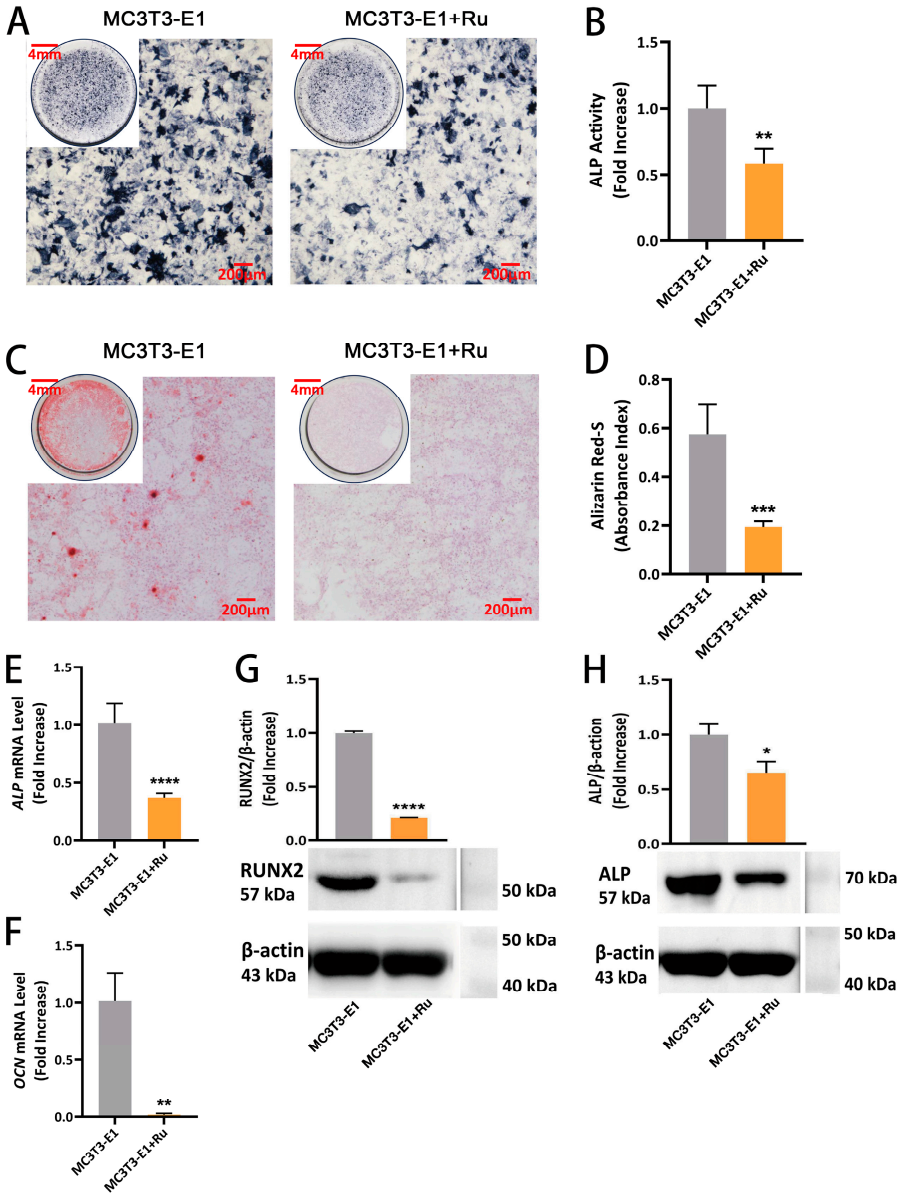

Figure 2: Inhibition of MCU function impairs the osteogenic function of MC3T3-E1 cells. (**A**) ALP staining images of MC3T3-E1 cells after 7-day osteogenic differentiation induction. Scale bar = 4 mm, Scale bar = 200 μm. (**B**) Quantitative analysis of ALP activity of MC3T3-E1 cells after 7-day osteogenic differentiation induction. (**C**) ARS staining of MC3T3-E1 cells after 14-day osteogenic differentiation induction. Scale bar = 4 mm, Scale bar = 200 μm. (**D**) Semi-quantitative analysis of alizarin red-S of MC3T3-E1 cells after 14-day osteogenic differentiation induction. (**E**,**F**) mRNA expression level of *ALP* and *OCN* gene in MC3T3-E1 cells after 7-day osteogenic differentiation induction. (**G**) The expression level and quantitative analysis of RUNX2 protein in MC3T3-E1 cells after 7-day osteogenic differentiation induction. (**H**) The expression level and quantitative analysis of ALP protein in MC3T3-E1 cells after 14-day osteogenic differentiation induction. Results are shown as means (of fold increase) ± SDs. $^{*}p < 0.05$, $^{**}p < 0.01$, $^{***}p < 0.001$ and $^{****}p < 0.0001$ versus the control group (MC3T3-E1), n = 5.

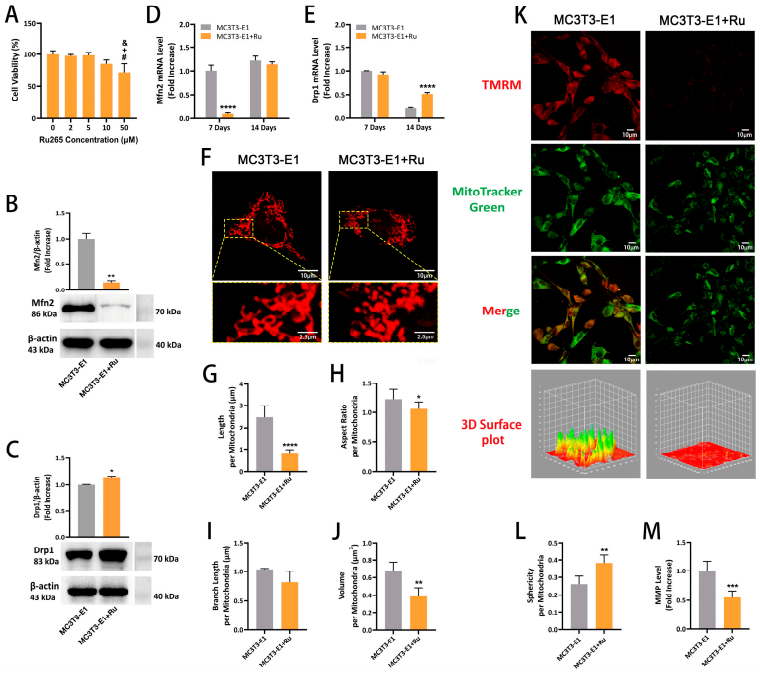

Figure 3: Inhibition of MCU function induces abnormal mitochondrial dynamics and mitochondrial dysfunction in MC3T3-E1 cells. (**A**) Cell activity determined by CCK-8 assay after 24 h of treatment using different concentrations of Ru265. (**B**) The expression level and quantitative analysis of Mfn2 protein in MC3T3-E1 cells after osteogenic differentiation induction for 7 days. (**C**) The expression level and quantitative analysis of Drp1 protein in MC3TE-E1 cells after osteogenic differentiation induction for 14 days. (**D**,**E**) The mRNA expression level of *Mfn2* and *Drp1* genes in MC3TE-E1 cells after osteogenic differentiation induction for 7 and 14 days. (**F**) Mitochondrial MitoTracker Red staining images of MC3T3-E1 cells and partial magnification (yellow dotted box). Scale bar = 2.5 μm, Scale bar = 10 μm. (**G**) Mitochondrial length analysis of MC3T3-E1 cells. (**H**) Mitochondrial aspect ratio analysis of MC3T3-E1 cells. (**I**) Mitochondrial branch length analysis of MC3T3-E1 cells. (**J**) Mitochondrial volume analysis of MC3T3-E1 cells. (**K**) Mitochondrial membrane potential (MMP) staining images and 3D surface plot of TMRM staining of MC3T3-E1 cells. Scale bar = 10 μm. (**L**) Mitochondrial sphericity analysis of MC3T3-E1 cells. (**M**) Quantitative analysis of MMP level. Results are shown as means (of fold increase) ± SDs. $^{\#}$, $^{+}$, and $^{\&}$ represent $p < 0.05$ when compared with 0 μM, 2 μM, and 5 μM groups, respectively. $^{*}p < 0.05$, $^{**}p < 0.01$, $^{***}p < 0.001$ and $^{****}p < 0.0001$ versus the control group (MC3T3-E1), n = 5.

To assess morphological consequences, we performed MitoTracker Red staining and 3D reconstruction of mitochondria [39]. MCU-inhibited cells exhibited shorter, rounder, and more fragmented mitochondria (Fig. 3F). Quantitative analyses confirmed reductions in mitochondrial length (Fig. 3G), aspect ratio (Fig. 3H), branch length (Fig. 3I), and volume (Fig. 3J), alongside increased sphericity (Fig. 3L), indicating fission dominance and network simplification. In addition, mitochondrial membrane potential (MMP) levels were measured via staining with TMRM, a fluorochrome sensitive to membrane potential. An obvious dissipation of MMP was detected in the MCU-inhibited group versus the control group (Fig. 3K,M). Given that MCU is the gateway that controls the inward flow of Ca^{2+} into mitochondria, we detected intra-mitochondrial Ca^{2+} using mitochondrial Ca^{2+}-specific fluorescent staining (Rhod-2 AM). When the MCU function was inhibited by Ru265, less Ca^{2+} flooded into the mitochondria, the fluorescence signal was weakened (Fig. A4A), and MMP was markedly decreased (Fig. A4B), indicating successful modeling. Furthermore, as a well-established agonist of MCU [40], spermine treatment (15 μmol/L) effectively rescued changes in Ca^{2+} and MMP

(Fig. A4A,B), and alleviated MCU-inhibition-mediated mitochondrial fission dominance and network simplification (Fig. A4C). The quantitative analyses of Ca^{2+} signal strength (Fig. A4D), mitochondrial average area (Fig. A4E), mitochondrial aspect ratio (Fig. A4F), mitochondrial form factor (Fig. A4G), mitochondrial branch length (Fig. A4H) and MMP (Fig. A4I), verified that the above changes were statistically different. These observations collectively indicate that mitochondrial dynamics and function were perturbed in cells subjected to MCU inhibition.

3.4 Gene Deletion of Mcu Leads to Compromised Osteogenic Potential and Bone Deficiency in Mice

To determine whether MCU function influences later stages of bone formation, we compared bone microstructure in wild-type (WT) and MCU global knockout (MCU KO) mice. Hematoxylin and eosin (H&E) staining revealed structural differences in femoral bone tissue, which were further quantified by micro-computed tomography (μCT) (Fig. 4A,B). *Mcu* knockout mice exhibited diminished trabecular bone number and thickness in the distal femur, as evidenced by significant reductions in BV/TV (Fig. 4C), Tb. N (Fig. 4D), and Tb. Th (Fig. 4E). Additionally, the MCU KO mice exhibited a notable increase in Tb. Sp (defined as the distance between adjacent trabeculae) (Fig. 4F). In the proximal tibia of MCU KO mice, trabecular bone number and thickness were also diminished (Fig. 4G,H), as reflected by significantly reduced BV/TV (Fig. 4I) and Tb. N (Fig. 4J). A similar but non-significant reduction was observed for Tb. Th (Fig. 4K), whereas Tb. Sp was notably increased (Fig. 4L).

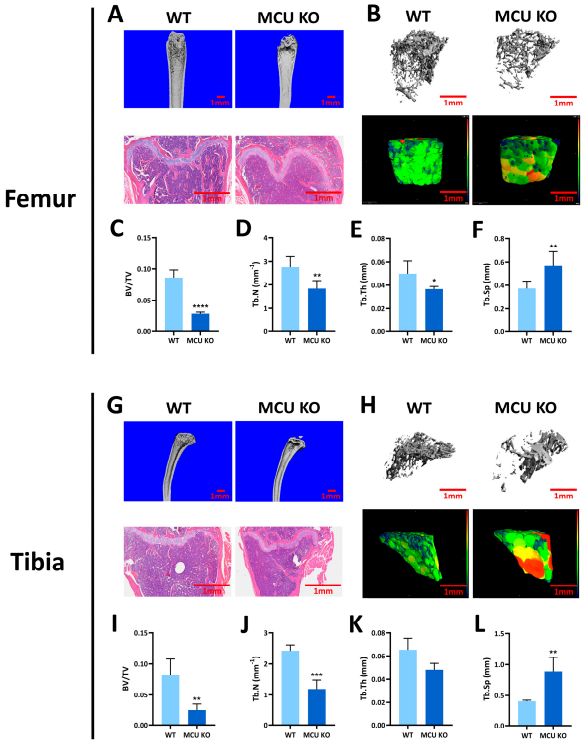

Figure 4: Gene deletion of *Mcu* leads to bone deficiency in mice. (**A**,**B**,**G**,**H**) Representative hematoxylin-eosin (HE) staining and micro-CT three-dimensional reconstruction images of femoral and tibial tissue of wildtype (WT) and *Mcu* gene knockout (MCU KO) mice. (**C**,**I**) Quantitative analysis of femoral and tibial bone volume fraction (BV/TV). (**D**,**J**) Quantitative analysis of femoral and tibial trabecular bone number (Tb.N). (**E**,**K**) Quantitative analysis of femoral and tibial trabecular bone thickness (Tb.Th). (**F**,**L**) Quantitative analysis of femoral and tibial trabecular bone separation (Tb.Sp). Scale bar = 1 mm. Results are shown as means ± SDs. $^{*}p < 0.05$, $^{**}p < 0.01$, $^{***}p < 0.001$ and $^{****}p < 0.0001$ versus the WT group, n = 4.

For further corroborating the role of MCU in osteogenic differentiation *in vivo*, we employed immunohistochemical (IHC) staining on femoral and tibial sections from wild-type (WT) mice and conventional *Mcu* gene knockout (MCU KO) mice. Expression of key osteogenic markers—RUNX2, OCN, ALP, and Bone morphogenetic protein (BMP2)—was markedly decreased in the femoral tissue of MCU KO mice compared to WT mice (Fig. 5A–D). We also observed a distinct reduction in osteoprotegerin (OPG), an inhibitor of osteoclast differentiation, in MCU-KO bone tissue (Fig. 5E). Consistent with diminished OPG levels, tartrate-resistant acid phosphatase (TRAP) staining revealed a pronounced increase in osteoclast number in MCU-KO mice (Fig. 5F). According to the above analysis, gene deletion of MCU leads to compromised osteogenic potential and bone deficiency in mice, which aligns with the *in vitro* findings.

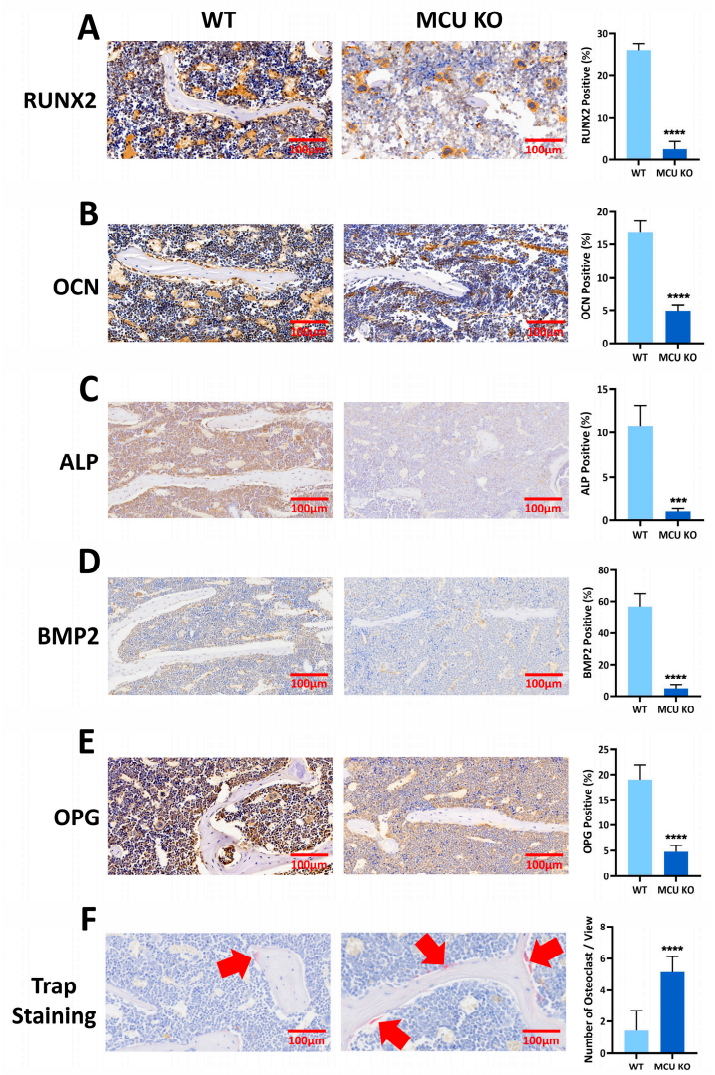

Figure 5: Gene deletion of *Mcu* leads to compromised osteogenic potential in mice. Immunohistochemical (IHC) staining and quantitative analysis of positive expression of (**A**) RUNX2, (**B**) OCN, (**C**) ALP, (**D**) BMP2, and (**E**) OPG expression in femoral tissues of WT and MCU KO mice (brown object indicates expression positive). (**F**) Tartrate-resistant acid phosphatase (Trap) staining (red arrow: osteoclasts, the cytoplasm is burgundy) and quantitative analysis of the number of osteoclasts in femoral tissues of WT and MCU KO mice; Scale bar, 100 μm. Results are shown as means ± SDs. ***$p < 0.001$ and ****$p < 0.0001$ versus the WT group, n = 6.

4 Discussion

MCU is a low-affinity, high-capacity calcium-selective channel located in the inner mitochondrial membrane. MCU-mediated modulation of mitochondrial calcium ions affects mitochondrial respiration, adenosine triphosphate (ATP) production, mitochondrial autophagy, mitochondrial apoptosis, and necrosis [41,42], playing vital roles in diverse mitochondria-mediated cellular physiological functions and pathological processes [43]. Recent studies have shown that MCU regulates diabetes [44], tumor metastasis and invasion [45], ischemia/reperfusion (I/R) injury [46], neuronal apoptosis [47], muscle atrophy [48], and abnormal lipid metabolism [13,49]. MCU modulates osteoclastogenesis and ovariectomized osteoporosis via RANKL-induced ROS production and NFATc1 activation through the P38 MAPK signaling pathway [50]. However, empirical investigations exploring the interplay between MCU and bone remain strikingly limited.

Our work utilized *Mcu* gene knockout mice and employed the MCU inhibitor Ru265 *in vitro* to carry out relevant experiments. Despite the importance of the MCU in physiological activities and pathological processes, research on modulating its calcium-uptake properties with agents is relatively limited. The most widely used MCU inhibitor is a ruthenium-based compound, Ru360, which inhibits MCU-mediated mitochondrial calcium uptake at nanomolar concentrations without affecting Na^+/Ca^{2+} exchange channels. The application of Ru360 *in vivo* has been shown to protect against ischemia-reperfusion injury in the rat heart [51]. However, the low cell permeability of Ru360 and the difficulty of purification and production limit its commercial application. A novel ruthenium-based compound, Ru265, has an MCU inhibitory effect more than 10-fold higher than that of Ru360, while exhibiting significantly enhanced cell permeability and better redox stability. Ru265 has been shown to confer protection against ischemia-reperfusion injury in neonatal rat ventricular myocytes [52]; maintains cortical neuronal respiration following lethal doses of oxygen-glucose deprivation and attenuates hypoxic/ischemic brain injury [53]; ablates nigericin-induced mitochondrial damage and NLRP3 inflammasome activation in LPS+12,13-DiHOME-primed macrophages [54]. Therefore, Ru265 has become an important chemical tool and potential therapeutic agent for the study of mitochondrial Ca^{2+} dysregulation-related diseases.

MCU is a heterodimeric protein complex that includes core MCU proteins [55] and several MCU function-related regulatory proteins, including MCU dominant negative beta subunit (MCUb) [56], Essential MCU Regulator (EMRE) [57], mitochondrial calcium uptake protein (MICU) family (MICU1, MICU2, MICU3) [36,58], MCU regulator 1 (MCUR1) [36], and solute carrier 25A23 (SLC25A23) [59], which are jointly involved in mitochondrial calcium ion transport [26]. In mouse tissues, MCU and MICU1 exhibit similar RNA expression [58]. MICU1 has an important role in MCU-dependent calcium ion transport, and Csordas et al. [34] found that MICU1 contributes to MCU activation under conditions of high intracellular calcium ion concentration. MICU1 downregulation reduces mitochondrial calcium ion content but does not significantly impair mitochondrial respiration or membrane potential [60]. We observed a concurrent increase in the mRNA expression of MCU, MICU1 and MCUb during the early osteogenic differentiation of MC3T3-E1 cells, and the specific inhibition of MCU function using Ru265 resulted in the upregulation of MCU, MICU1 and MCUb gene expression, suggesting that MICU1 may act synergistically with MCU to allow calcium ions into mitochondria, and that inhibition of mitochondrial calcium uptake could lead to compensatory upregulation of MCU and MICU1 genes. MCUb is a dominant-negative isoform of MCU. The incorporation of MCUb into the channel complex reduces the overall calcium conductance efficiency of the channel. The upregulation of MCU, MICU1, and MCUb following functional inhibition of MCU is likely a multi-layered compensatory transcriptional reprogramming initiated by the cell to cope with prolonged suppression of mitochondrial calcium uptake. The root cause lies in Ru265's ability to bypass the MICU1 gatekeeping barrier, functionally mimicking a MICU1-deficient state and thereby triggering a

negative feedback loop aimed at re-establishing calcium homeostasis [61,62]. Within this framework, MCUb upregulation can be interpreted as an "enhanced gatekeeping" strategy to structurally inhibit channel activity further [63]. Concurrently, the off-target effects of Ru265 may indirectly amplify these gene expression changes by perturbing cytosolic calcium signaling [64].

Recent evidence suggests that oxygen consumption rate and intracellular ATP content are significantly upregulated during osteogenic differentiation, suggesting that mitochondrial energy metabolism is involved in the specific differentiation of mesenchymal stem cells (MSCs) [65–67]. Studies have reported impaired mitochondrial oxidative phosphorylation in MSCs following the use of respiratory chain complex inhibitors (e.g., antimycin A), ATP synthase inhibitors (e.g., oligomycin), or uncoupling agents (e.g., FCCP), resulting in the inhibition of osteogenic differentiation [65,67,68]. Osteoblast differentiation and mineralization are important stages of bone formation [69]. RUNX2 is a major transcription factor that determines the osteoblast lineage and is closely associated with the regulation of osteoblast differentiation, matrix production, and mineralization [70]. RUNX2 is considered to be a major regulatory gene for osteogenesis and is able to induce the expression of osteoblast-specific genes, including OCN and Osteopontin (OPN) [71]. In addition, the expression and activity of ALP during osteogenic differentiation indicate differentiation of mesenchymal stromal cells (MSCs) towards osteoblasts [72]. In the present study, we used MCU-specific inhibitor Ru265 to explore the regulatory role of MCU on osteogenic differentiation of MC3T3-E1 cells, and the results showed that MCU function inhibition decreased the expression level of the osteogenic gene RUNX2 in MC3T3-E1 cells, significantly reduced ALP expression, significantly decreased extracellular matrix calcium nodule production, and significantly diminished osteogenic differentiation. Our results demonstrate that MCU is critical for the osteogenic function of MC3T3-E1 cells, regulating both differentiation and mineralization. Consequently, Ru265 emerges as a potent tool for investigating mitochondrial mechanisms in bone metabolism and associated disorders.

In the latest investigations, findings have come to light that MCU plays a critical regulatory role in many physiological functions, therapeutic processes, and pathological processes by mediating alterations in mitochondrial dynamics, including modulation of dendritic mitochondrial morphology and synaptic plasticity [30], sodium butyrate induced colorectal cancer cell apoptosis [31], intestinal ischemia–reperfusion injury [32] and pulmonary vascular remodeling in pulmonary hypertension [73]. Mitochondrial dynamics are closely regulated by key proteins such as Mfn2 and Drp1 [38]. It has been reported that mitochondrial morphology undergoes dynamic changes from a tubular network to a fragmented structure during osteogenic differentiation of MC3T3-E1 cells, suggesting that mitochondrial morphological changes may be a new indicator of osteoblast differentiation [74]. Our results revealed that MCU function inhibition could increase Drp1 expression and decrease Mfn2 expression during osteogenic differentiation of MC3T3-E1 cells, leading to excessive mitochondrial fission and mitochondrial fragmentation, resulting in the imbalance of mitochondrial dynamics. It is suggested that MCU can regulate mitochondrial dynamics during osteogenic differentiation of pre-osteoblasts through Drp1 and Mfn2. The present study showed that abnormal MCU function reduces MMP, induces Drp1 overexpression, and suppresses mitofusion-2 (Mfn2) expression in MC3T3-E1 cells, indicating that MCU may regulate the cell osteogenic differentiation through mitochondrial dynamics.

MCU is closely associated with cellular life activities and the pathological status of the body through the regulation of mitochondrial calcium homeostasis. Current *in vivo* studies on MCU mainly focus on cardiovascular diseases: studies have reported that upregulation of MCU gene expression by the calcium-regulated protein kinase CaMKIIδB maintains calcium homeostasis and cardiomyocyte viability to reverse stress-induced pathological cardiac remodeling [75]. However, studies on the regulatory effects of MCU on bone structures have rarely been reported. In the present work, microstructural and histological

analysis of bone tissue of *Mcu* gene knockout mice revealed less bone formation, poor bone microstructure, significantly decreased expression of osteogenesis-related proteins, and increased osteoclast genesis. It is further confirmed that MCU plays a key regulatory role in osteogenic differentiation and bone remodeling in the body (Fig. 6).

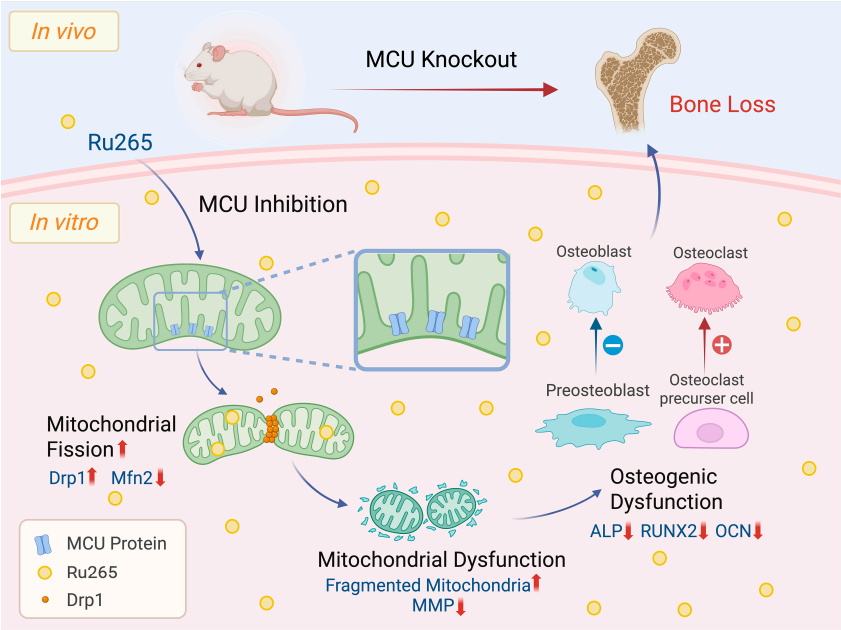

Figure 6: Schematic diagram depicting MCU inhibition-induced disrupted bone remodeling and impaired osteogenic function via aberrant mitochondrial dynamics and mitochondrial function. The upward arrows represent upregulation, and the downward arrows represent downregulation. The "+" represents promotion of cell differentiation, and the "−" represents inhibition of cell differentiation. The figure was created in BioRender. Fu, X. (2025) https://BioRender.com/dxfj9ve and published with permission.

5 Conclusion

In summary, we demonstrate that inhibition of MCU notably impacts osteogenic function by regulating mitochondrial function and dynamics through key proteins, including Mfn2 and Drp1, which consequently result in bone deficiency. Accordingly, our work provides a novel theoretical basis for the study of bone regeneration and repair therapies targeting MCU and key proteins of mitochondrial function and dynamics.

Acknowledgement: Not applicable.

Funding Statement: This work was supported by the National Natural Science Foundation of China (82370935, 81870802), Sichuan Province Science and Technology Support Program Grant (2023YFS0244), Sichuan Science and Technology Program (2025ZNSFSC0768), Clinical Research Project Funded by West China Hospital of Stomatology Sichuan University (LCYJ-MS-202302), The Key Research and Development Support Program of the Chengdu Science and Technology Bureau (2024-YF05-00505-SN), and Research Project on Graduate Education and Teaching Reform of Sichuan University (GSSCU2024105).

Author Contributions: The authors confirm contribution to the paper as follows: Conceptualization, Xueqi Gan; methodology, Xueqi Gan; validation, Xinliang Fu and Wen Du; formal analysis, Xinliang Fu, Wen Du, Tao Li, Ngai-Fung Ruan and Huiling Ling; data curation, Xinliang Fu, Yifei Shen, Xingbo Wu, Ziqi Qin and Xiting Zhu; writing—original draft preparation, Xinliang Fu and Wen Du; writing—review and editing, Xinliang Fu, Wen Du, Tao Li, Yifei Shen, Ngai-Fung Ruan, Huiling Ling, Xingbo Wu, Ziqi Qin, Xiting Zhu and Xueqi Gan; visualization,

Xinliang Fu, Wen Du and Xueqi Gan; supervision, Xueqi Gan; project administration, Xueqi Gan; funding acquisition, Wen Du and Xueqi Gan. All authors reviewed and approved the final version of the manuscript.

Availability of Data and Materials: All data supporting the results of this study are included within the article. Further inquiries can be directed to the corresponding author.

Ethics Approval: The study included animal subjects and approved by the Research Ethics Committee of West China Hospital of Stomatology, Sichuan University (Approval No. WCHSIRB-D-2022-271, date of approval: 24 February 2022).

Conflicts of Interest: The authors declare no conflicts of interest.

Abbreviations

MCU	Mitochondrial calcium uniporter
BMSCs	Bone marrow mesenchymal stem cells
MC3T3-E1	Mouse embryo osteoblast precursor cell
Drp1	Dynamin-related protein 1
Mfn2	Mitofusion-2
MMP	Mitochondrial membrane potential
AGEs	Advanced glycation end products
ROS	Reactive Oxygen Species
DAMPs	Damage-associated molecular patterns
mtDNA	Mitochondrial DNA
MSCs	Mesenchymal stem cells
HSCs	Hematopoietic stem cells
PBS	Phosphate buffer saline
FBS	Fetal bovine serum
αMEM	Alpha minimum essential medium
MICU1	Mitochondrial calcium uptake 1
ATP	Adenosine triphosphate
IMM	Inner mitochondrial membrane
EMRE	Essential MCU Regulator
ALP	Alkaline phosphatase
ARS	Alizarin-red S
MCUR1	Mitochondrial calcium uniporter regulator 1
SLC25A23	Solute carrier 25A23
RUNX2	Runt-related transcription factor 2
OCN	Osteocalcin
OPN	Osteopontin
RANK	Receptor activator of nuclear factor kappa B
RANKL	Receptor activator of nuclear factor kappa B ligand
OPG	Osteoprotegerin
PVDF	Polyvinylidene Fluoride
LSCM	Laser scanning confocal microscope
BV/TV	Bone volume/Total volume
Tb.N	Trabecular number
Tb.Th	Trabecular thickness
Tb.Sp	Trabecular separation/spacing
OCN	Osteocalcin
BMP2	Bone morphogenetic protein
HE	Hematoxylin-eosin
IHC	Immunohistochemistry
Trap	Tartrate-resistant acid phosphatase

Appendix A

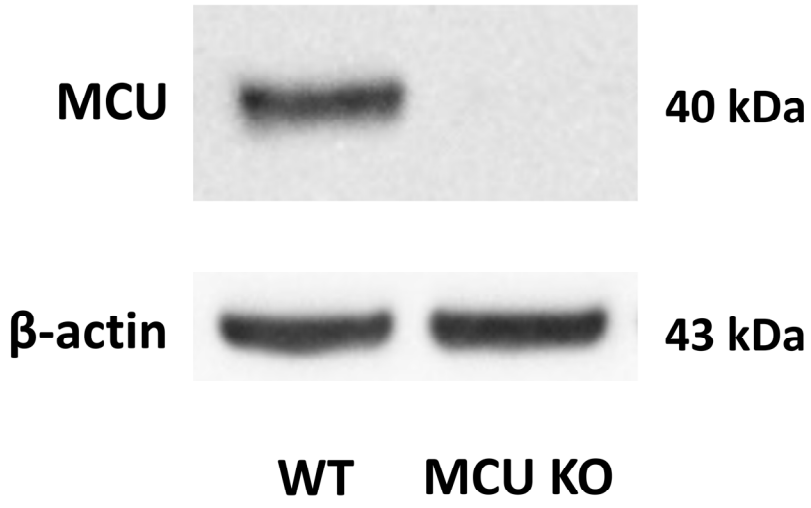

Figure A1: The expression of MCU protein in bone tissues of wild-type (WT) and MCU global knockout (MCU KO) mice.

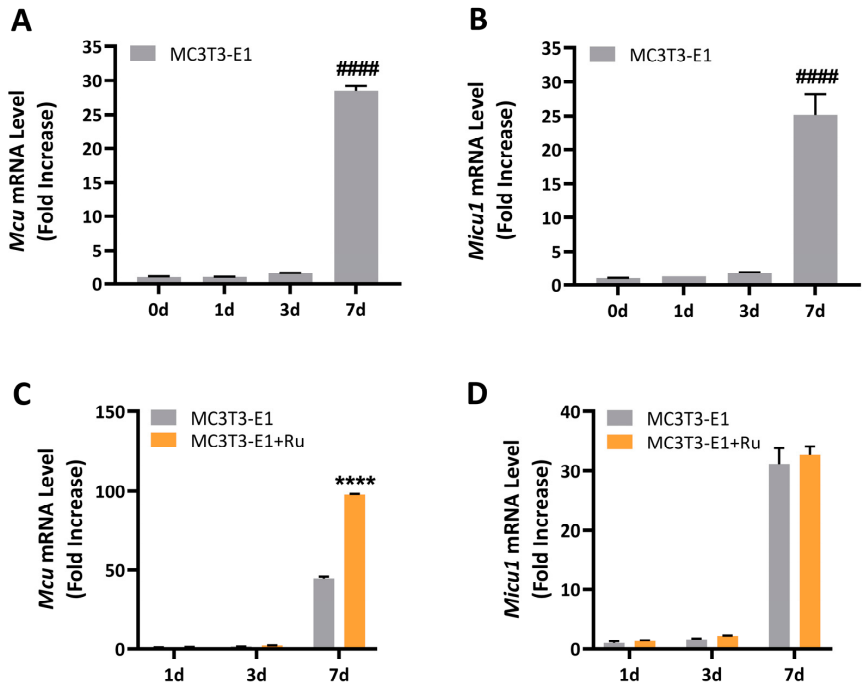

Figure A2: The effect of abnormal MCU function on the expression of *Mcu* and *Micu1* gene during 7 days of osteogenic differentiation of MC3T3-E1 cells. (**A**,**B**) mRNA expression level of *Mcu* and *Micu1* gene of MC3T3-E1 cells after osteogenic differentiation induction for 0 d, 1 d, 3 d, and 7 d. (**C**,**D**) mRNA expression level of *Mcu* and *Micu1* gene of the control group (MC3T3-E1) and the MCU function inhibition group (MC3T3-E1 + Ru) after osteogenic differentiation induction for 1 d, 3 d, and 7 d. Results are shown as means of fold increase ± SDs. $^{\#\#\#\#}p < 0.0001$ versus the undifferentiated group (0 d); $^{****}p < 0.0001$ versus the control group (MC3T3-E1), n = 5.

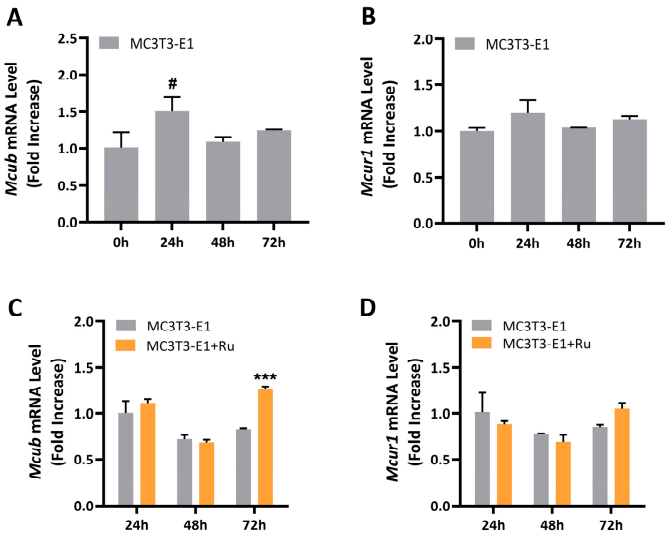

Figure A3: The effect of abnormal MCU function on the expression of *Mcub* and *Mcur1* gene in the early stage of osteogenic differentiation of MC3T3-E1 cells. (**A**,**B**) mRNA expression level of *Mcub* and *Mcur1* gene of MC3T3-E1 cells after osteogenic differentiation induction for 0 h, 24 h, 48 h, and 72 h. (**C**,**D**) mRNA expression level of *Mcub* and *Mcur1* gene of the control group (MC3T3-E1) and the MCU function inhibition group (MC3T3-E1 + Ru) after osteogenic differentiation induction for 0 h, 24 h, 48 h, and 72 h. Results are shown as means of fold increase ± SDs. $^{\#}p < 0.05$ versus the undifferentiated group (0 h); $^{***}p < 0.001$ versus the control group (MC3T3-E1), n = 5.

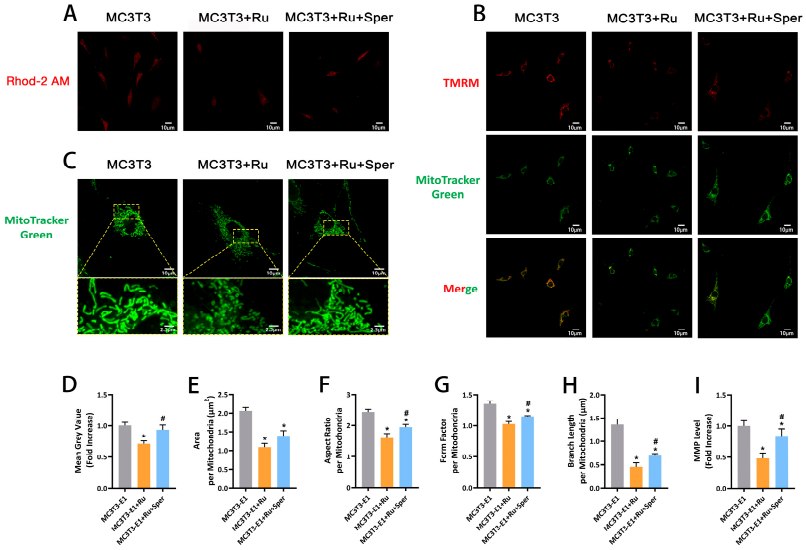

Figure A4: Effect of spermine on MCU inhibition-induced abnormal mitochondrial dynamics and mitochondrial dysfunction in MC3T3-E1 cells. (**A**) Observation of mitochondrial Ca^{2+} signaling by laser confocal microscopy. (**B**) Detection of mitochondrial membrane potential (MMP) levels. (**C**) Mitochondrial MitoTracker Green staining images of MC3T3-E1 cells and partial magnification (yellow dotted box). Scale bar = 2.5 μm, Scale bar = 10 μm. (**D**) The quantitative analysis of Ca^{2+} signal strength. Mitochondrial average (**E**) area, (**F**) aspect ratio, (**G**) form factor, and (**H**) branch length of MC3T3-E1 cells. (**I**) The quantitative analysis of MMP levels. Results are shown as means (of fold increase) ± SDs. * and # represent $p < 0.05$ when compared with MC3T3-E1 and MC3T3-E1 + Ru group, respectively, n = 5.

References

1. Plotkin LI, Bruzzaniti A. Molecular signaling in bone cells: Regulation of cell differentiation and survival. Adv Protein Chem Struct Biol. 2019:237–81. [CrossRef].
2. Huang Y, Li X, Jing Q, Zhang Q, Huang C. BMP-2 inhibits the inflammatory response and promotes bone formation in rats with femoral fracture by activating the AMPK signaling pathway. Biocell. 2025;49(11):2195–216. [CrossRef].
3. Nunnari J, Suomalainen A. Mitochondria: In sickness and in health. Cell. 2012;148(6):1145–59. [CrossRef].
4. Șerban M, Toader C, Covache-Busuioc RA. The redox revolution in brain medicine: Targeting oxidative stress with AI, multi-omics and mitochondrial therapies for the precision eradication of neurodegeneration. Int J Mol Sci. 2025;26(15):7498. [CrossRef].
5. Franco-Obregón A. Magnetic mitohormesis: A non-invasive therapy for inflammatory disorders? Biocell. 2023;47(2):239–44. [CrossRef].
6. Ru JY, Wang YF. Osteocyte apoptosis: The roles and key molecular mechanisms in resorption-related bone diseases. Cell Death Dis. 2020;11:846. [CrossRef].
7. Zhu X, Qin Z, Zhou M, Li C, Jing J, Ye W, et al. The role of mitochondrial permeability transition in bone metabolism, bone healing, and bone diseases. Biomolecules. 2024;14(10):1318. [CrossRef].
8. Dobson PF, Dennis EP, Hipps D, Reeve A, Laude A, Bradshaw C, et al. Mitochondrial dysfunction impairs osteogenesis, increases osteoclast activity, and accelerates age related bone loss. Sci Rep. 2020;10(1):11643. [CrossRef].
9. Tang S, Tang T, Gao G, Wei Q, Sun K, Huang W. Bone marrow mesenchymal stem cell-derived exosomes inhibit chondrocyte apoptosis and the expression of MMPs by regulating Drp1-mediated mitophagy. Acta Histochem. 2021;123(8):151796. [CrossRef].
10. Sun X, Mao Y, Dai P, Li X, Gu W, Wang H, et al. Mitochondrial dysfunction is involved in the aggravation of periodontitis by diabetes. J Clin Periodontol. 2017;44(5):463–71. [CrossRef].
11. Ding Y, Yang H, Wang Y, Chen J, Ji Z, Sun H. Sirtuin 3 is required for osteogenic differentiation through maintenance of PGC-1α-SOD2-mediated regulation of mitochondrial function. Int J Biol Sci. 2017;13(2):254–64. [CrossRef].
12. Guo Y, Jia X, Cui Y, Song Y, Wang S, Geng Y, et al. Sirt3-mediated mitophagy regulates AGEs-induced BMSCs senescence and senile osteoporosis. Redox Biol. 2021;41:101915. [CrossRef].
13. Ambrosi TH, Scialdone A, Graja A, Gohlke S, Jank AM, Bocian C, et al. Adipocyte accumulation in the bone marrow during obesity and aging impairs stem cell-based hematopoietic and bone regeneration. Cell Stem Cell. 2017;20(6):771–84.e6. [CrossRef].
14. Machiela E, Liontis T, Dues DJ, Rudich PD, Traa A, Wyman L, et al. Disruption of mitochondrial dynamics increases stress resistance through activation of multiple stress response pathways. FASEB J. 2020;34(6):8475–92. [CrossRef].
15. Peace MR, Madide T, Sibiya N. Drug-induced insulin sensitivity impairments: Potential involvement of disturbed mitochondrial dynamics and mitophagy pathways. Biocell. 2025;49(11):2069–91. [CrossRef].
16. Ballard A, Zeng R, Zarei A, Shao C, Cox L, Yan H, et al. The tethering function of mitofusin2 controls osteoclast differentiation by modulating the Ca^{2+}-NFATc1 axis. J Biol Chem. 2020;295(19):6629–40. [CrossRef].
17. Jeong S, Seong JH, Kang JH, Lee DS, Yim M. Dynamin-related protein 1 positively regulates osteoclast differentiation and bone loss. FEBS Lett. 2021;595(1):58–67. [CrossRef].
18. Jung S, Kwon JO, Kim MK, Song MK, Kim B, Lee ZH, et al. Mitofusin 2, a mitochondria-ER tethering protein, facilitates osteoclastogenesis by regulating the calcium-calcineurin-NFATc1 axis. Biochem Biophys Res Commun. 2019;516(1):202–8. [CrossRef].
19. He Y, Gan X, Zhang L, Liu B, Zhu Z, Li T, et al. $CoCl_2$ induces apoptosis *via* a ROS-dependent pathway and Drp1-mediated mitochondria fission in periodontal ligament stem cells. Am J Physiol Cell Physiol. 2018;315(3):C389–97. [CrossRef].
20. Zhang L, Gan X, He Y, Zhu Z, Zhu J, Yu H. Drp1-dependent mitochondrial fission mediates osteogenic dysfunction in inflammation through elevated production of reactive oxygen species. PLoS One. 2017;12(4):e0175262. [CrossRef].

21. Wang L, Huang X, Dai T, Xie J, Lv QX, Hou Y, et al. The role of mitochondrial dynamics in the TiO_2 nanotube-accelerated osteogenic differentiation of MC3T3-E1 cells. Biochem Biophys Res Commun. 2021;535:33–8. [CrossRef].
22. Gan X, Huang S, Liu Y, Yan SS, Yu H. The potential role of damage-associated molecular patterns derived from mitochondria in osteocyte apoptosis and bone remodeling. Bone. 2014;62:67–8. [CrossRef].
23. Mao H, Chen W, Chen L, Li L. Potential role of mitochondria-associated endoplasmic reticulum membrane proteins in diseases. Biochem Pharmacol. 2022;199:115011. [CrossRef].
24. Zanfardino P, Amati A, Perrone M, Petruzzella V. The balance of MFN2 and OPA1 in mitochondrial dynamics, cellular homeostasis, and disease. Biomolecules. 2025;15(3):433. [CrossRef].
25. Wang FS, Kuo CW, Ko JY, Chen YS, Wang SY, Ke HJ, et al. Irisin mitigates oxidative stress, chondrocyte dysfunction and osteoarthritis development through regulating mitochondrial integrity and autophagy. Antioxidants. 2020;9(9):810. [CrossRef].
26. Feno S, Rizzuto R, Raffaello A, Vecellio Reane D. The molecular complexity of the mitochondrial calcium uniporter. Cell Calcium. 2021;93:102322. [CrossRef].
27. Pallafacchina G, Zanin S, Rizzuto R. From the identification to the dissection of the physiological role of the mitochondrial calcium uniporter: An ongoing story. Biomolecules. 2021;11(6):786. [CrossRef].
28. Joseph LC, Reyes MV, Homan EA, Gowen B, Avula UMR, Goulbourne CN, et al. The mitochondrial calcium uniporter promotes arrhythmias caused by high-fat diet. Sci Rep. 2021;11:17808. [CrossRef].
29. Li X, Zhao J, Lv Q, Tian Y, Zhang L, Liu T. Electroacupuncture alleviates multifidus muscle injury by modulating mitochondrial function and Ca^{2+} uptake. Anat Rec. 2023;306(12):3060–72. [CrossRef].
30. Pannoni KE, Fischer QS, Tarannum R, Cawley ML, Alsalman MM, Acosta N, et al. MCU expression in hippocampal CA2 neurons modulates dendritic mitochondrial morphology and synaptic plasticity. Sci Rep. 2025;15:4540. [CrossRef].
31. Qin Y, Liu L, Luo S, He H, Sun X, Zhang Q, et al. Sodium butyrate induces colorectal cancer cell apoptosis *via* the MCU/Drp1 pathway. Int Immunopharmacol. 2025;161:115052. [CrossRef].
32. Kadier T, Zhang YG, Jing YX, Weng ZY, Liao SS, Luo J, et al. MCU inhibition protects against intestinal ischemia–reperfusion by inhibiting Drp1-dependent mitochondrial fission. Free Radic Biol Med. 2024;221:111–24. [CrossRef].
33. Pan X, Liu J, Nguyen T, Liu C, Sun J, Teng Y, et al. The physiological role of mitochondrial calcium revealed by mice lacking the mitochondrial calcium uniporter. Nat Cell Biol. 2013;15(12):1464–72. [CrossRef].
34. Csordás G, Golenár T, Seifert EL, Kamer KJ, Sancak Y, Perocchi F, et al. MICU1 controls both the threshold and cooperative activation of the mitochondrial Ca^{2+} uniporter. Cell Metab. 2013;17(6):976–87. [CrossRef].
35. Garg V, Suzuki J, Paranjpe I, Unsulangi T, Boyman L, Milescu LS, et al. The mechanism of MICU-dependent gating of the mitochondrial Ca^{2+} uniporter. eLife. 2021;10:e69312. [CrossRef].
36. Mallilankaraman K, Cárdenas C, Doonan PJ, Chandramoorthy HC, Irrinki KM, Golenár T, et al. MCUR1 is an essential component of mitochondrial Ca^{2+} uptake that regulates cellular metabolism. Nat Cell Biol. 2012;14:1336–43. Erratum in: Nat Cell Biol. 2013;123(2):15. [CrossRef].
37. Bruno SR, Kumar A, Mark ZF, Chandrasekaran R, Nakada E, Chamberlain N, et al. DRP1-mediated mitochondrial fission regulates lung epithelial response to allergen. Int J Mol Sci. 2021;22(20):11125. [CrossRef].
38. Tilokani L, Nagashima S, Paupe V, Prudent J. Mitochondrial dynamics: Overview of molecular mechanisms. Essays Biochem. 2018;62(3):341–60. [CrossRef].
39. Li W, Deng Y, Feng B, Mak KK. Mst1/2 kinases modulate glucose uptake for osteoblast differentiation and bone formation. J Bone Miner Res. 2018;33(6):1183–95. [CrossRef].
40. Xiong YB, Huang WY, Ling X, Zhou S, Wang XX, Li XL, et al. Mitochondrial calcium uniporter promotes kidney aging in mice through inducing mitochondrial calcium-mediated renal tubular cell senescence. Acta Pharmacol Sin. 2024;45(10):2149–62. [CrossRef].
41. East DA, Campanella M. Ca^{2+} in quality control: An unresolved riddle critical to autophagy and mitophagy. Autophagy. 2013;9(11):1710–9. [CrossRef].
42. Gottlieb RA, Bernstein D. Mitochondrial remodeling: Rearranging, recycling, and reprogramming. Cell Calcium. 2016;60(2):88–101. [CrossRef].

43. Murgia M, Rizzuto R. Molecular diversity and pleiotropic role of the mitochondrial calcium uniporter. Cell Calcium. 2015;58(1):11–7. [CrossRef].
44. Wang CH, Wei YH. Role of mitochondrial dysfunction and dysregulation of Ca^{2+} homeostasis in the pathophysiology of insulin resistance and type 2 diabetes. J Biomed Sci. 2017;24(1):70. [CrossRef].
45. Stejerean-Todoran I, Zimmermann K, Gibhardt CS, Vultur A, Ickes C, Shannan B, et al. MCU controls melanoma progression through a redox-controlled phenotype switch. EMBO Rep. 2022;23(11):e54746. [CrossRef].
46. Wu XY, Wang R, Zhang Q, Liu T, Liu JY, Xu XS, et al. Aging aggravated liver ischemia and reperfusion injury by promoting oxidized mtDNA mediated-macrophage pyroptosis through acetylated MCU-dependent calcium uptake. Cell Death Discov. 2025;11:449. [CrossRef].
47. Yang X, Chen Y, Zheng G, Nie Q, Zhang P. Mitochondrial calcium uniporter (MCU)-mediated calcium overload in psychoactive drug neurotoxicity: From pathogenesis to therapeutic targets. Int J Mol Sci. 2025;26(10):4732. [CrossRef].
48. Butera G, Vecellio Reane D, Canato M, Pietrangelo L, Boncompagni S, Protasi F, et al. Parvalbumin affects skeletal muscle trophism through modulation of mitochondrial calcium uptake. Cell Rep. 2021;35(5):109087. [CrossRef].
49. Flicker D, Sancak Y, Mick E, Goldberger O, Mootha VK. Exploring the *in vivo* role of the mitochondrial calcium uniporter in brown fat bioenergetics. Cell Rep. 2019;27(5):1364–75.e5. [CrossRef].
50. Wang Y, Li X, Zhou S, Li J, Zhu Y, Wang Q, et al. MCU inhibitor ruthenium red alleviates the osteoclastogenesis and ovariectomized osteoporosis *via* suppressing RANKL-induced ROS production and NFATc1 activation through P38 MAPK signaling pathway. Oxid Med Cell Longev. 2022;2022:7727006. [CrossRef].
51. Guan L, Che Z, Meng X, Yu Y, Li M, Yu Z, et al. MCU Up-regulation contributes to myocardial ischemia-reperfusion Injury through calpain/OPA-1-mediated mitochondrial fusion/mitophagy Inhibition. J Cell Mol Med. 2019;23(11):7830–43. [CrossRef].
52. Woods JJ, Nemani N, Shanmughapriya S, Kumar A, Zhang M, Nathan SR, et al. A selective and cell-permeable mitochondrial calcium uniporter (MCU) inhibitor preserves mitochondrial bioenergetics after hypoxia/reoxygenation injury. ACS Cent Sci. 2019;5(1):153–66. [CrossRef].
53. Novorolsky RJ, Nichols M, Kim JS, Pavlov EV, J Woods J, Wilson JJ, et al. The cell-permeable mitochondrial calcium uniporter inhibitor Ru265 preserves cortical neuron respiration after lethal oxygen glucose deprivation and reduces hypoxic/ischemic brain injury. J Cereb Blood Flow Metab. 2020;40(6):1172–81. [CrossRef].
54. Valencia R, Kranrod JW, Fang L, Soliman AM, Azer B, Clemente-Casares X, et al. Linoleic acid-derived diol 12, 13-DiHOME enhances NLRP3 inflammasome activation in macrophages. FASEB J. 2024;38(13):e23748. [CrossRef].
55. De Stefani D, Raffaello A, Teardo E, Szabò I, Rizzuto R. A forty-kilodalton protein of the inner membrane is the mitochondrial calcium uniporter. Nature. 2011;476(7360):336–40. [CrossRef].
56. Raffaello A, De Stefani D, Sabbadin D, Teardo E, Merli G, Picard A, et al. The mitochondrial calcium uniporter is a multimer that can include a dominant-negative pore-forming subunit. EMBO J. 2013;32(17):2362–76. [CrossRef].
57. Sancak Y, Markhard AL, Kitami T, Kovács-Bogdán E, Kamer KJ, Udeshi ND, et al. EMRE is an essential component of the mitochondrial calcium uniporter complex. Science. 2013;342(6164):1379–82. [CrossRef].
58. Kamer KJ, Mootha VK. MICU1 and MICU2 play nonredundant roles in the regulation of the mitochondrial calcium uniporter. EMBO Rep. 2014;15(3):299–307. [CrossRef].
59. Hoffman NE, Chandramoorthy HC, Shanmughapriya S, Zhang XQ, Vallem S, Doonan PJ, et al. SLC25A23 augments mitochondrial Ca^{2+} uptake, interacts with MCU, and induces oxidative stress-mediated cell death. Mol Biol Cell. 2014;25(6):936–47. [CrossRef].
60. Perocchi F, Gohil VM, Girgis HS, Bao XR, McCombs JE, Palmer AE, et al. MICU1 encodes a mitochondrial EF hand protein required for Ca^{2+} uptake. Nature. 2010;467(7313):291–6. [CrossRef].
61. Rodríguez-Prados M, Huang KT, Márta K, Paillard M, Csordás G, Joseph SK, et al. MICU1 controls the sensitivity of the mitochondrial Ca^{2+} uniporter to activators and inhibitors. Cell Chem Biol. 2023;30(6):606–17.e4. [CrossRef].
62. Rodríguez-Prados M, Berezhnaya E, Castromonte MT, Menezes-Filho SL, Paillard M, Hajnóczky G. MICU1 occludes the mitochondrial calcium uniporter in divalent-free conditions. Proc Natl Acad Sci U S A. 2023;120(19):1–10. [CrossRef].
63. Noble M, Colussi DM, Junop M, Stathopulos PB. The MCU and MCUb amino-terminal domains tightly interact: Mechanisms for low conductance assembly of the mitochondrial calcium uniporter complex. iScience. 2024;27(5):109699. [CrossRef].

64. Xu P, Swain S, Novorolsky RJ, Garcia E, Huang Z, Snutch TP, et al. The mitochondrial calcium uniporter inhibitor Ru265 increases neuronal excitability and reduces neurotransmission *via* off-target effects. Br J Pharmacol. 2024;181(18):3503–26. [CrossRef].
65. Shares BH, Busch M, White N, Shum L, Eliseev RA. Active mitochondria support osteogenic differentiation by stimulating β-catenin acetylation. J Biol Chem. 2018;293(41):16019–27. [CrossRef].
66. Forni MF, Peloggia J, Trudeau K, Shirihai O, Kowaltowski AJ. Murine mesenchymal stem cell commitment to differentiation is regulated by mitochondrial dynamics. Stem Cells. 2016;34(3):743–55. [CrossRef].
67. Gao J, Feng Z, Wang X, Zeng M, Liu J, Han S, et al. SIRT3/SOD2 maintains osteoblast differentiation and bone formation by regulating mitochondrial stress. Cell Death Differ. 2018;25(2):229–40. [CrossRef].
68. Chen CT, Shih YV, Kuo TK, Lee OK, Wei YH. Coordinated changes of mitochondrial biogenesis and antioxidant enzymes during osteogenic differentiation of human mesenchymal stem cells. Stem Cells. 2008;26(4):960–8. [CrossRef].
69. Sanches MLR, Tokuhara CK, de Oliveira FA, Ventura T, de Souza Pessoa A, Iano FG, et al. Crosstalk between adipocytes and osteoblasts in regulating bone differentiation. Mol Cell Endocrinol. 2026;616:112764. [CrossRef].
70. Sun M, Chi G, Li P, Lv S, Xu J, Xu Z, et al. Effects of matrix stiffness on the morphology, adhesion, proliferation and osteogenic differentiation of mesenchymal stem cells. Int J Med Sci. 2018;15(3):257–68. [CrossRef].
71. Jeong JH, Choi JY. Interrelationship of Runx2 and estrogen pathway in skeletal tissues. BMB Rep. 2011;44(10):613–8. [CrossRef].
72. Capulli M, Paone R, Rucci N. Osteoblast and osteocyte: Games without frontiers. Arch Biochem Biophys. 2014;561:3–12. [CrossRef].
73. Chen H, Qiu YX, Xie YF, Chen X, Xiang YY, Zhang HL, et al. Redox switch C674 in SERCA2 triggers Ca^{2+}-calcineurin-MCU-Drp1 cascade and pulmonary vascular remodeling. Free Radic Biol Med. 2026;244:380–94. [CrossRef].
74. Arakaki N, Yamashita A, Niimi S, Yamazaki T. Involvement of reactive oxygen species in osteoblastic differentiation of MC3T3-E1 cells accompanied by mitochondrial morphological dynamics. Biomed Res. 2013;34(3):161–6. [CrossRef].
75. Wang P, Xu S, Xu J, Xin Y, Lu Y, Zhang H, et al. Elevated MCU expression by CaMKIIδB limits pathological cardiac remodeling. Circulation. 2022;145(14):1067–83. [CrossRef].